

Automatika

Journal for Control, Measurement, Electronics, Computing and Communications



ISSN: (Print) (Online) Journal homepage: <https://www.tandfonline.com/loi/taut20>

Single-phase front-end bridgeless modified Landsman-Canonical Switching Cell PFC converter for arc welding applications

J. Gnanavadivel & M. Shunmathi

To cite this article: J. Gnanavadivel & M. Shunmathi (2023) Single-phase front-end bridgeless modified Landsman-Canonical Switching Cell PFC converter for arc welding applications, *Automatika*, 64:1, 104-113, DOI: [10.1080/00051144.2022.2109743](https://doi.org/10.1080/00051144.2022.2109743)

To link to this article: <https://doi.org/10.1080/00051144.2022.2109743>



© 2022 The Author(s). Published by Informa UK Limited, trading as Taylor & Francis Group



Published online: 09 Aug 2022.



Submit your article to this journal [↗](#)



Article views: 446



View related articles [↗](#)



View Crossmark data [↗](#)



Single-phase front-end bridgeless modified Landsman-Canonical Switching Cell PFC converter for arc welding applications

J. Gnanavadeivel and M. Shunmathi

Department of Electrical and Electronics Engineering, Mepco Schlenk Engineering College, Sivakasi, Tamilnadu, India

ABSTRACT

This research paper proposes an enhanced power quality in bridgeless modified Landsman-Canonical switching cell (BMLCSC) converter used for arc welding power supplies. This proposed converter topology is presented for circuit component reduction to eliminate the need for a diode bridge rectifier and input filter to make the circuit more compact. The proposed converter is operated on discontinuous conduction mode (DCM). A closed loop PI control circuit with a single voltage sensor is utilized to achieve load regulation, line regulation with high efficiency and quick response. The exploratory performance of preferred framework is simulated using Matlab/Simulink and validated with a hardware prototype of 100 W, 48 V.

ARTICLE HISTORY

Received 19 January 2022
Accepted 29 July 2022

KEYWORDS

Arc welding; power factor correction; modified Landsman-CSC converter; discontinuous conduction mode; Total harmonic distortion

1. Introduction

Nowadays, many industries broadly use arc welding power supplies. Attributable to high efficiency are becoming main stream in various low and medium power applications. Among these previous developments different alloys are used for lower production cost, higher electrical conductivity and good mechanical properties. It made the researchers to design simplified AC-DC converters with modest size and cost. Good arc welding process ensures good weld seam quality and posses quick response [1–4]. Traditional, AC-DC converter usually includes the bridge rectifier circuit and a large capacitor to attain DC voltage. This converter unavoidably presents a high source current distortion, bringing about an enormous measure of low-power quality. The attractive features of this front-end PFC converter topology find their application in arc welding. The merits of this converter include good power quality, high PF, and low inrush current under different load conditions. Moreover, the PQ indices of the PFC converter meet the specifications of an International Standard IEC 61000-3-2 [2–5]. Numerous converters for arc welding power supplies were compared on the basis of the aforementioned attributes and are reported in the literature [1–5].

Previously mentioned PFC configurations furnish the acceptable current harmonic limit as well as power factor. Various passive wave shaping circuits are presented [6] for the improvement of the power factor. The investigations on single-phase DBR with an LC filter at the input side involve two sensing loops and

make the system more complicated [7]. Initially, the buck and boost power converters are used to improve the input power factor. Here, a discontinuous capacitor voltage mode buck converter with an input filter is described. However, DCVM operation incurs demerits of high peak current on the switch and high voltage ripples at the output side. Single-input multiple-output boost PFC converter is operated in CCM and DCM used for various load applications [8]. Single-stage PFC-based LED driver configurations have been reported in [9]. Buck-boost PFC topology offers better power quality but it encompasses an EMI filter that results in high overshoot transients and less efficiency.

In recent years many researchers focus on distinctive converter topologies, such as Sepic, Zeta, Cuk, CSC, and Landsman, widely used for medium power applications and give more recommendations for power quality improvement [10–14]. Non-isolated Zeta converter-based dimming concept in the LED lighting system for power quality improvement is illustrated in [10]. This converter is designed to operate on full load and experiences input source current THD of around 8.52%. It also necessitates filter capacitance and dimming circuit which makes the overall system more complex and expensive. GA-tuned PI controller for Sepic power factor correction converter is reported in [11]. Here, an average current control method is deployed that requires two voltage sensors and one current sensor resulting in a complex controller design. A conventional cuk converter for enhancing the power quality in

BLDC motor drive is presented in [12]. This converter exhibits sluggish response with limited dynamic range control.

The front-end canonical switching cell converter-fed BLDC motor for input wave shaping is presented in [13]. The requirement of the filter circuit is tedious and the overall system size and cost will be higher. The Landsman converter-fed BLDC motor drive for a medium power application is shown in [14]. The purpose of the DC filter is used to reduce the harmonic content in the input source current. The landsman PFC converter-based LED Driver for wide area prediction applications is illustrated in [15]. The main drawback of the system involves the negative output voltage which necessitates the use of an amplifier circuit. For modified Landsman converter in [16] suffers source current THD ranges between 2.4% and 8.4% for a wide range of variation in DC voltage.

A huge amount of losses occurs due to the presence of a diode bridge rectifier in previously mentioned converter topologies. Therefore, many researchers are attracted to the bridgeless topologies that reduce conduction losses and high inrush current. The BL-buck converter is inappropriate for arc welding power supply applications because of its limited output voltage range. In this study, the buck–boost configurations of the Sepic, Zeta, and Cuk converters were found to have higher switching losses and power losses [17–22]. In this literature, a PFC-based bridgeless Luo converter-fed BLDC motor drive is mentioned in [23]. This negative output Luo converter resulted in the source current THD being 9.9% at rated load conditions. The DCM mode of operation is preferred in the positive output Luo converter. Also this topology adds an input filter that ended up with a high complex circuit design and low efficiency [24].

This study describes the use of a BL-CSC configuration for BLDC motor drive [25]. Here, the input filter arrangement is mandatory for the suppression of source current harmonics which is the limitations of the system as well as the total size of the system is high. For rated voltage, THD goes beyond 5% even with the usage of an input AC filter. In this paper [26], the BL-Landsman converter with a single sensor circuit and stress reduction were mentioned to improve power quality. The BL-modified Landsman converter topology is employed to power an EV battery charger. This converter differs by reconfiguring the inductors on the input and output sides, as reported in [27]. Due to the continuous conduction mode of the input inductances, the converter seems to have a low output ripple current.

This research work proposes a Bridgeless modified Landsman–Canonical Switching Cell (BMLCSC) converter to improve power quality in arc welding applications. In comparison to [27], the preferred converter that operates on DCM mode possesses fewer

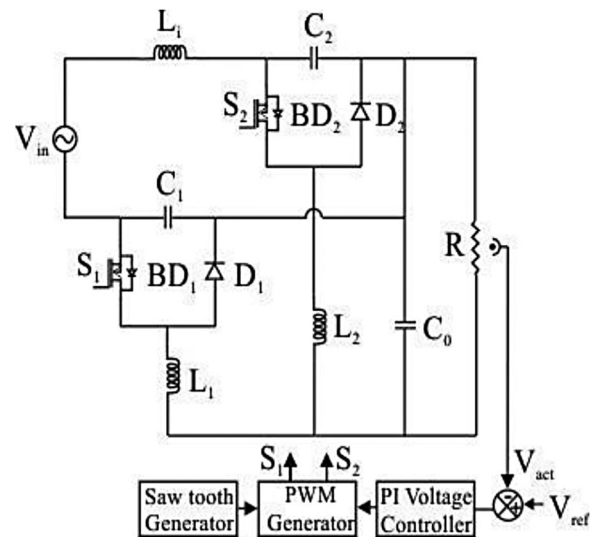


Figure 1. Symbolic representation of a BMLCSC converter circuit.

components, no input filter, and provides a positive output voltage with a simple controller arrangement. Consequently, the modified converter also has some merits, such as simple, cost-effective, and high efficiency. Furthermore, even for the wide range of source voltage variation and load power variation the preferred converter maintains the power quality on the source side.

2. Working of bridgeless modified landsman-CSC converter

The proposed converter includes two switching devices (S_1 , S_2), two intermediate capacitors (C_1 , C_2), three inductors (L_1 , L_2 , L_i), two diodes (D_1 , D_2), one filter capacitor (C_0), and resistive load. During the positive half cycle, circuit components involved in conduction for three modes are switch S_1 , the body diode of S_2 , L_1 , L_2 , L_i , C_1 , and C_0 . On the other hand, switch S_2 , the body diode of switches S_1 , L_1 , L_2 , L_i , C_2 , and C_0 for the negative half cycle. Figure 1 shows the proposed converter includes two switching devices (S_1 , S_2), two intermediate capacitors (C_1 , C_2), three inductors (L_1 , L_2 , L_i), two diodes (D_1 , D_2), filter capacitor (C_0), resistive load.

2.1. Mode 1

During the positive half cycle, switch S_1 is activated, as shown in Figure 2. The source inductance L_i and the body diode of switch S_2 begins to conduct. L_2 inductor responds to the releasing energy stored in the L_1 inductor. The stored energy in the intermediate capacitor C_1 is released towards the load and output capacitor C_0 .

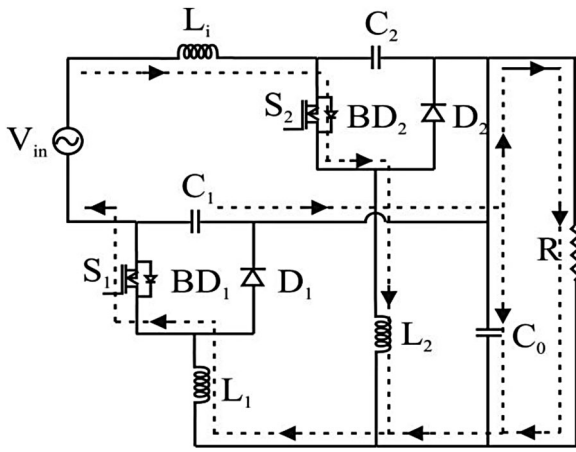


Figure 2. Mode-1 circuit.

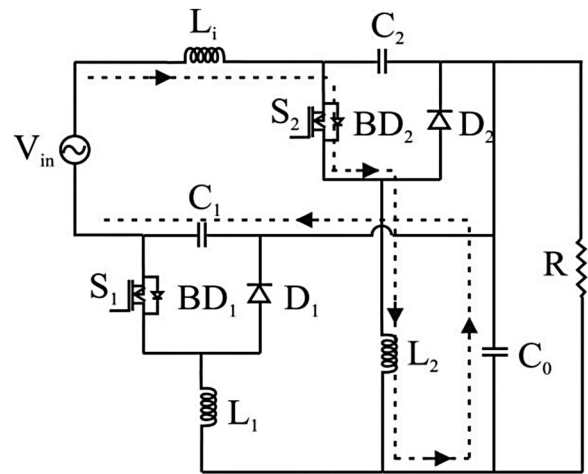


Figure 4. Mode-3 circuit.

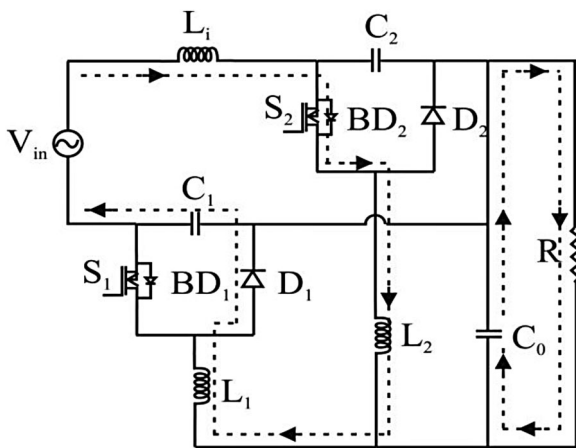


Figure 3. Mode-2 circuit.

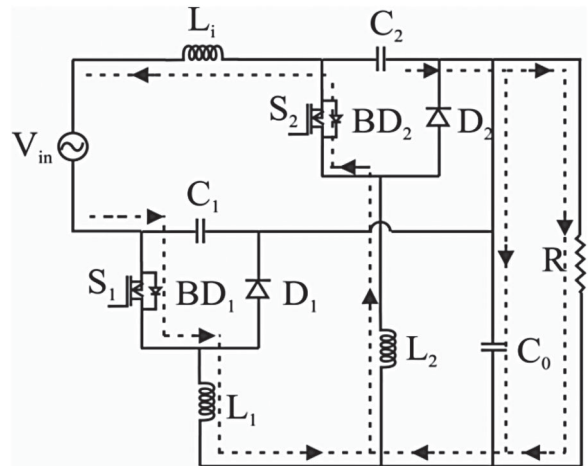


Figure 5. Mode-4 circuit.

2.2. Mode 2

During this mode, both switches are in off condition, as shown in Figure 3. The current conduction takes place through the body diode of switch S_2 and diode D_1 . L_i discharges its energy to inductor L_2 . In addition, inductor L_1 starts to release its energy to intermediate capacitor C_1 . The energy is supplied to the load via the output capacitor C_0 .

2.3. Mode 3

The input inductor L_1 completely discharges its energy and operates in discontinuous mode during the positive half cycle, shown in Figure 4. The intermediate capacitor C_1 stores the energy saved in the inductor L_2 . Current flows through the input inductor L_i and the body diode of switch S_2 when the supply voltage V_{in} is applied. The load receives energy from the output capacitor C_0 . Figure 8 shows the switching waveforms during the positive half cycle.

2.4. Mode 4

When the switch S_2 is operated during the negative half cycle, the source inductor L_i was being charged. The discharging current of inductor L_1 charges up the inductor L_2 . To meet the load demand and charge up the output capacitor, intermediate capacitor C_2 begins to release its stored energy, as shown in Figure 5.

2.5. Mode 5

In this mode of operation, both switches are off conditions, as shown in Figure 6. The current flows through the diode D_2 and the body diode of switch S_1 . Inductors L_i and L_2 start discharging their stored energy and charge the intermediate capacitor C_2 . L_1 gets charged up due to the supply voltage V_{in} . The output capacitor C_0 provides the power required by the load.

2.6. Mode 6

In this last mode of operation, during the negative half cycle, both switches remain off, as shown in Figure 7.

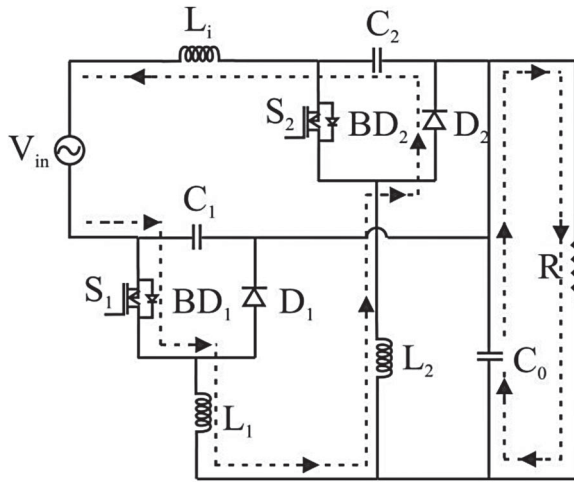


Figure 6. Mode-5 circuit.

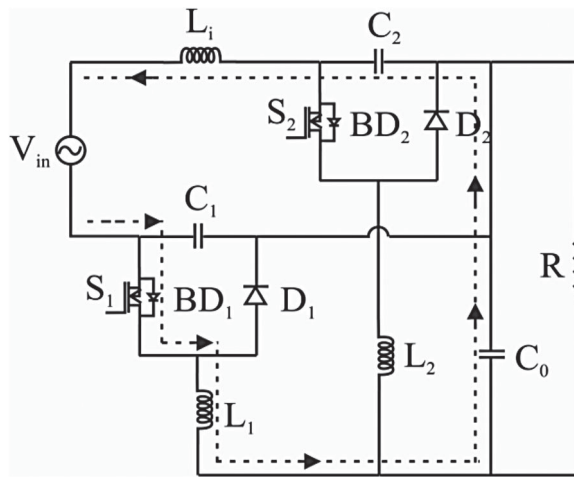


Figure 7. Mode-6 circuit.

After discharging its stored energy completely, inductor L_2 goes to DCM operation. Intermediate Capacitor C_2 is getting charged due to the flow of discharging current of input inductor L_i . Inductor L_i is getting charged due to the flow of supply current via the body diode of switch S_1 . The load demand is supplied by output capacitor C_0 . Figure 9 shows the switching waveforms during the negative half cycle.

3. Converter design

The working of the inductors (L_1 and L_2) in both half cycles on discontinuous conduction mode is taken into consideration when designing the front-end modified converter of 100 W and 48 V from which, the design values of intermediate capacitors C_1 and C_2 , intermediate inductors L_1 and L_2 , input inductor L_i and output capacitor C_0 are determined. The frequency of switching (f_s) is set to 20 kHz.

The input inductor inductance was calculated using a 20% ripple (δ) current allowed with a minimum source voltage. V_{dc} denotes the proposed converter's dc

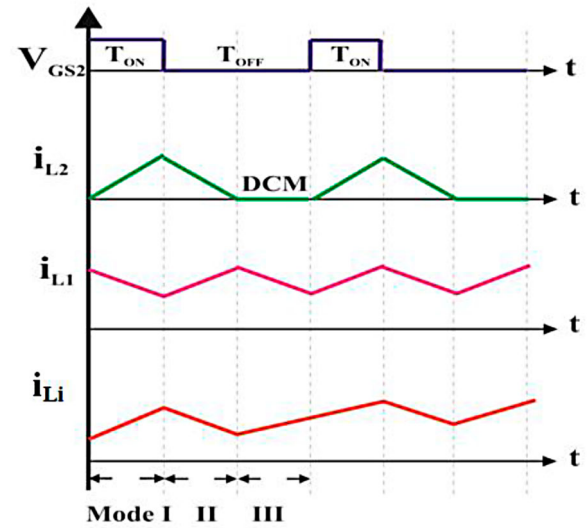


Figure 8. Positive half cycle switching operation.

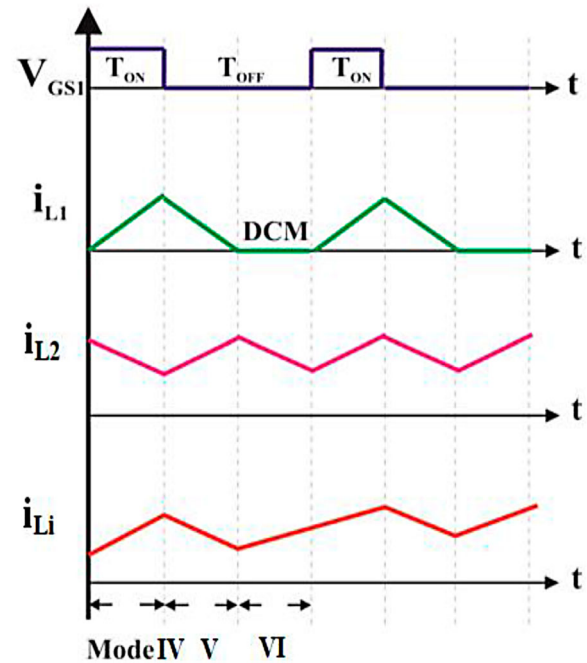


Figure 9. Negative half cycle switching operation.

link voltage.

$$L_i = \frac{1}{\delta f_s} \left(\frac{V_{in}^2}{P_i} \right) X \frac{V_{dc \max}}{V_{dc \max} + V_{in}} = 5.2 \text{mH} \quad (1)$$

The selected input inductance value for continuous conduction mode operation of the input inductor is 5 mH. The value of two intermediate inductors L_1 and L_2 , which operate in the boundary conduction mode, is determined.

$$\begin{aligned} L_{1,2} &= \left(\frac{V_{s \min}^2}{P_{\max}} \right) \frac{1}{2f_s} X \frac{V_{dc \max}}{V_{dc \max} + \sqrt{2}V_{in \min}} \\ &= 554.52 \mu\text{H} \end{aligned} \quad (2)$$

The value of the intermediate inductors is taken as $100 \mu\text{H}$ to make sure it works on discontinuous conduction mode. Whereas, the intermediate capacitors operate in continuous conduction mode. Here, the ripple voltage of the capacitor is assumed to be 20%.

$$C_{1,2} = \frac{P_{\max}}{\eta\sqrt{2}V_{in\max}f_sX(V_{dc\max} + \sqrt{2}V_{in\max})} = 304.63\text{nF} \quad (3)$$

For, providing continuous conduction capacitor values are chosen as 600 nF.

For a ripple voltage (κ) of 2% of $V_{dc\max}$, the output capacitor value is calculated as follows.

$$C_0 = \frac{P_{\max}}{2\omega\kappa V_{dc\max}^2} = 1849.53\mu\text{F} \quad (4)$$

As a result, a $2500 \mu\text{F}$ output capacitor is effective for this arc welding application.

4. Modified converter modeling

The power factor correction converter is designed using state space parameters, such as intermediate capacitor voltage, input inductor current and intermediate inductor current, and output capacitor voltage (V_0). The output voltage is controlled by the proposed BMLCSC converter, which includes control logic and a PI voltage controller. By comparing the reference value of 48 V with the actual output voltage with the help of the comparator and the error value is sent to the controller. A sawtooth waveform generator is used to perform the PI controller's output and generate the appropriate gate pulses, which are then required by power switches. The state equations obtained from the state matrix are used to design the propounded converter. The state vector is denoted by the X matrix, the input matrix by B_n , the output matrix by C, and the state matrix by A_n .

$$X^1 = A_n X + B_n V_s \quad (5)$$

$$V_0 = CX \quad (6)$$

$$\begin{bmatrix} \frac{di_{Li}}{dt} \\ \frac{dV_{C1}}{dt} \\ \frac{di_{L1}}{dt} \\ \frac{dV_{C2}}{dt} \\ \frac{di_{L2}}{dt} \\ \frac{dV_{C0}}{dt} \end{bmatrix} = \begin{bmatrix} 0 & 0 & 0 & 0 & 0 & 0 \\ 0 & 0 & \frac{-1}{C_1} & \frac{1}{C_1} & 0 & 0 \\ 0 & 0 & 0 & \frac{1}{L_1} & 0 & 0 \\ 0 & \frac{-1}{C_2} & \frac{1}{C_2} & 0 & 0 & 0 \\ 0 & 0 & 0 & 0 & \frac{1}{L_2} & 0 \\ 0 & 0 & 0 & \frac{1}{C_0} & 0 & \frac{1}{RC_0} \end{bmatrix}$$

$$\times \begin{bmatrix} i_{Li} \\ V_{C1} \\ i_{L1} \\ V_{C2} \\ i_{L2} \\ V_{C0} \end{bmatrix} + \begin{bmatrix} \frac{1}{L_i} \\ 0 \\ 0 \\ 0 \\ 0 \\ 0 \end{bmatrix} [V_{in}] \quad (7)$$

$$\begin{bmatrix} \frac{di_{Li}}{dt} \\ \frac{dV_{C1}}{dt} \\ \frac{di_{L1}}{dt} \\ \frac{dV_{C2}}{dt} \\ \frac{di_{L2}}{dt} \\ \frac{dV_{C0}}{dt} \end{bmatrix} = \begin{bmatrix} 0 & 0 & 0 & 0 & \frac{-1}{L_i} & 0 \\ 0 & 0 & 0 & \frac{1}{C_1} & 0 & 0 \\ 0 & \frac{1}{L_1} & 0 & 0 & 0 & 0 \\ 0 & 0 & \frac{1}{C_2} & \frac{-1}{C_2} & 0 & 0 \\ 0 & \frac{1}{L_2} & 0 & 0 & 0 & 0 \\ 0 & 0 & 0 & \frac{1}{C_0} & 0 & \frac{1}{RC_0} \end{bmatrix}$$

$$\times \begin{bmatrix} i_{Li} \\ V_{C1} \\ i_{L1} \\ V_{C2} \\ i_{L2} \\ V_{C0} \end{bmatrix} + \begin{bmatrix} \frac{1}{L_i} \\ 0 \\ 0 \\ 0 \\ 0 \\ 0 \end{bmatrix} [V_{in}] \quad (8)$$

$$\begin{bmatrix} \frac{di_{Li}}{dt} \\ \frac{dV_{C1}}{dt} \\ \frac{di_{L1}}{dt} \\ \frac{dV_{C2}}{dt} \\ \frac{di_{L2}}{dt} \\ \frac{dV_{C0}}{dt} \end{bmatrix} = \begin{bmatrix} 0 & 0 & 0 & 0 & \frac{-1}{L_i} & 0 \\ 0 & 0 & 0 & \frac{1}{C_1} & \frac{-1}{C_1} & 0 \\ 0 & 0 & \frac{1}{L_1} & 0 & 0 & 0 \\ 0 & 0 & \frac{-1}{C_2} & 0 & 0 & 0 \\ 0 & \frac{-1}{L_2} & 0 & 0 & 0 & 0 \\ 0 & 0 & 0 & \frac{1}{C_0} & 0 & \frac{1}{RC_0} \end{bmatrix}$$

$$\times \begin{bmatrix} i_{Li} \\ V_{C1} \\ i_{L1} \\ V_{C2} \\ i_{L2} \\ V_{C0} \end{bmatrix} + \begin{bmatrix} \frac{1}{L_i} \\ 0 \\ 0 \\ 0 \\ 0 \\ 0 \end{bmatrix} [V_{in}] \quad (9)$$

There are 3 major modes in this case, and the state space equations for each can be found here (9). With the help of the input matrix and the state matrix all the mathematical formulations are enumerated for this proposed converter, as portrayed in Equation (16).

The duty ratios $d_1 = 0.05$ and $d_2 = 0.15$ are for the switch and diode on time periods, respectively.

$$A = A_1 d_1 + A_2(1 - d_1) + A_3(1 - d_1 - d_2) \quad (10)$$

$$B = B_1 d_1 + B_2(1 - d_1) + B_3(1 - d_1 - d_2) \quad (11)$$

$$C = [0 \ 0 \ 0 \ 1] \quad (12)$$

$$D = [0] \quad (13)$$

$$G(s) = \frac{V_0(s)}{V_{in}(s)} = C(sI - A)^{-1}B \quad (14)$$

$$G(s) = \frac{6.39e^{-15}s^3 + 1.924e^6s^2 - 3.629e^8s - 1.412e^{16}}{s^6 + 429.63s^5 - 5.2837e^7s^4 + 8.927e^5s^3 - 3.251e^{10}s^2 - 1.694e^3s + 1.638e^{12}} \quad (15)$$

$$G_c(s) = K_p + \frac{K_i}{s} \quad (16)$$

Figures 10 and 11 depict the bode plot and step response of the proposed BMLCSC converter for stability, respectively.

5. Simulation outcomes

Figure 12 shows the supply voltage and source current waveforms acquired under rated load conditions. The output voltage waveform of the modified converter is depicted in Figure 13. The visual representation of a sudden change in load at $T = 1$ sec could be seen in Figure 14. Figure 15 shows the FFT analysis of source current THD at under-rated load conditions for the BMLCSC converter. Total harmonic distortion is estimated to be around 1.67%. Figure 16 depicts the results of the designed converter when the supply voltage varies. For supply voltage variations of 90 to 230 V, the power factor differs from 0.9947 to 0.9999, and THD values range from 1.48% to 3.10%. The effectiveness of the propounded converter for different load variations is shown in Figure 17. Here, THD values range from 1.67% to 2.4% with input power changes varying from 0.995 to 0.9999. Figure 18 depicts the comparison of conventional landsman converter and BL-Landsman-CSC converter under wide variation in load power. Figure 19 shows the total harmonic distortion of the traditional converter and modified converter under varying load powers. In addition, the BL converter based on the conventional buck-boost and Cuk, Sepic arrangement is not observed to be very efficient, as shown in Figure 20, when compared to other similar BL topologies, the preferred modified converter has been proven to be more efficient.

6. Proposed PFC converter hardware set-up

Figure 21 shows the hardware set-up of the BMLCSC converter. This converter is designed for output power

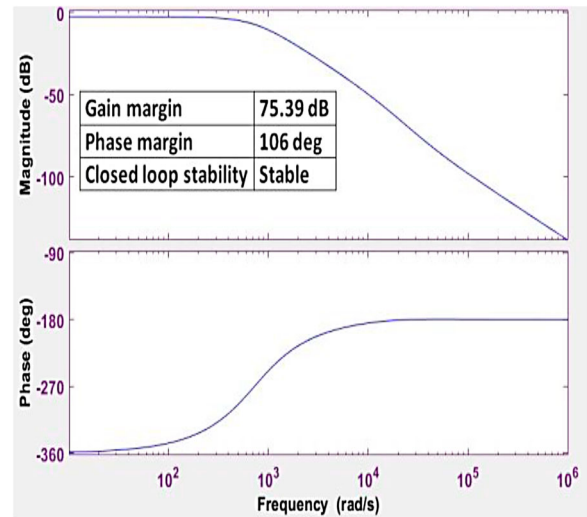


Figure 10. Bode plot.

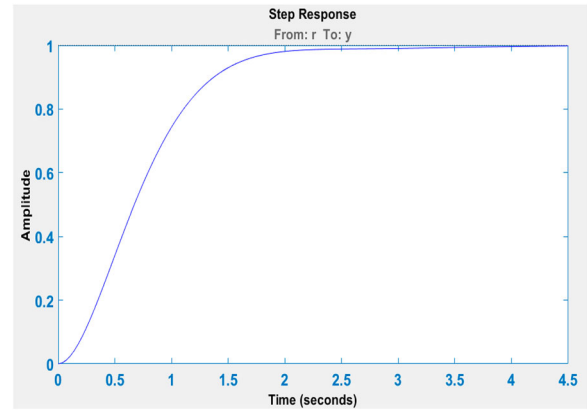


Figure 11. Step response.

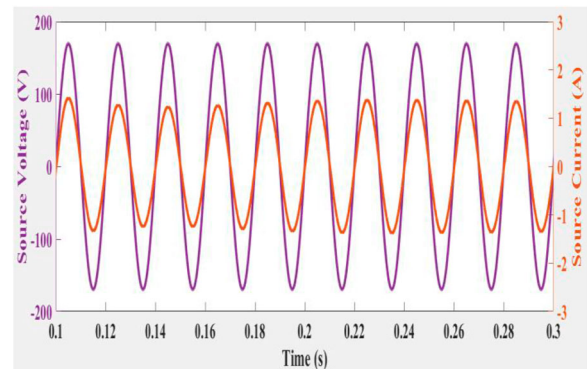


Figure 12. Waveforms of input voltage and source current.

and voltage of 100 W, 48 V. For output voltage $V_0(n)$, V_{LS} is the control signal generated by the controller and V_{err} is the error signal.

$$V_{LS}(n) = V_{LS}(n-1) + K_P\{V_{err}(n) - V_{err}(n-1)\} + K_I V_{err}(n) \quad (17)$$

$$V_{err}(n) = V_0 * (n) - V_0(n) \quad (18)$$

where n denotes the n th sampling moment.

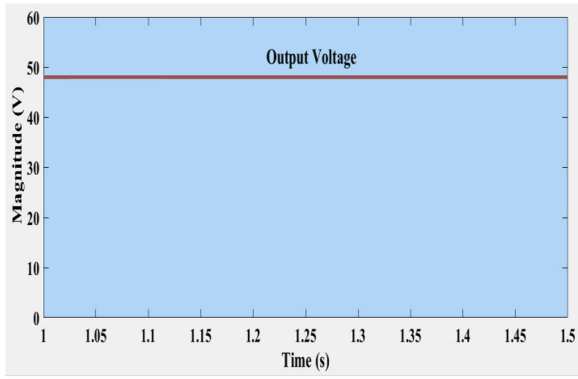


Figure 13. Output voltage waveform.

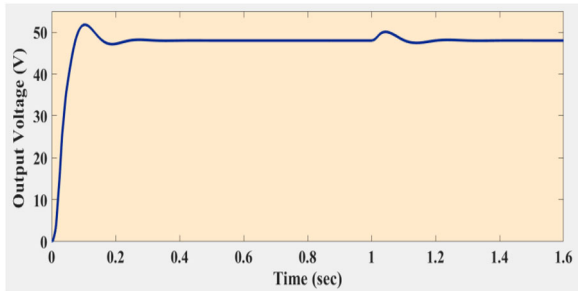


Figure 14. For the change in load condition.

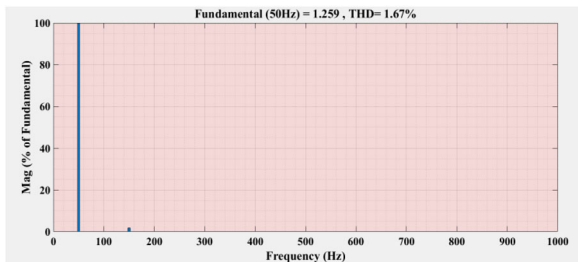


Figure 15. FFT waveform.

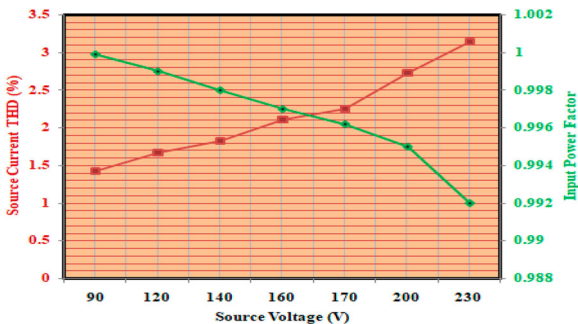


Figure 16. Performance analysis of the BL-Landsman-CSC converter for source voltage variation.

The PI voltage controller is built with a PIC micro-controller that generates gating signals for switches in the proper sequence to obtain the desired output.

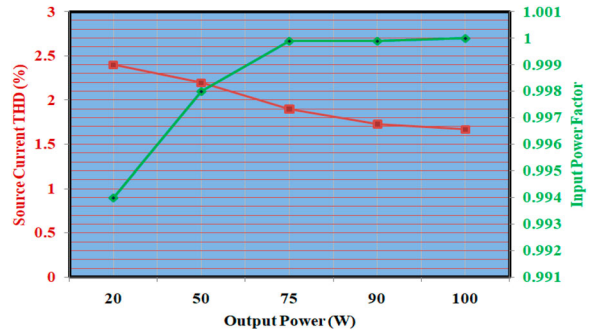


Figure 17. Performance analysis of the BL-Landsman-CSC converter for variation of load power.

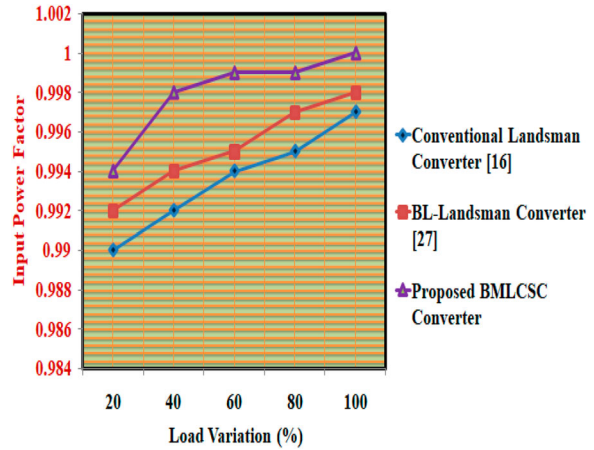


Figure 18. Comparative analysis of power factor variation.

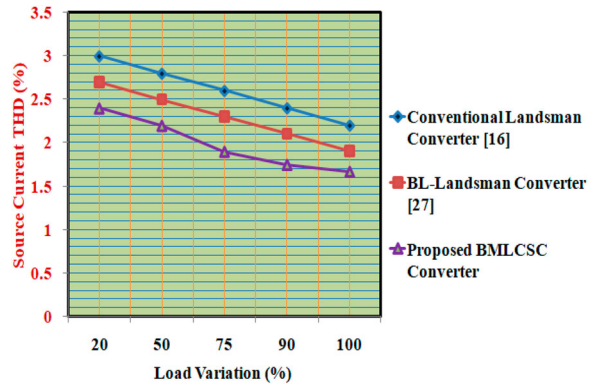


Figure 19. Comparative analysis of source current THD.

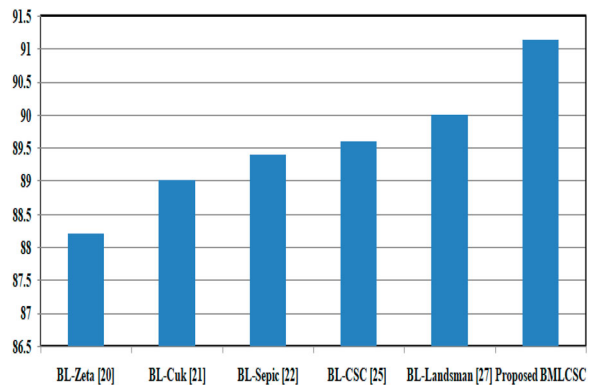


Figure 20. Comparative study evaluation of efficiency.

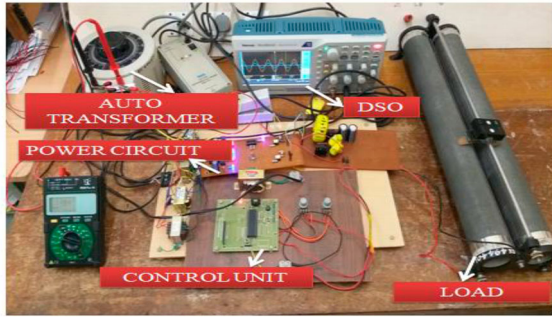
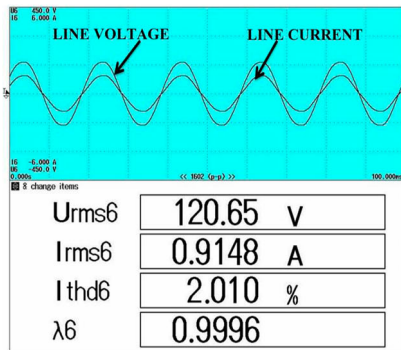
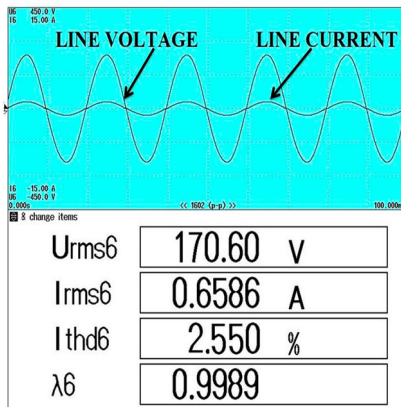


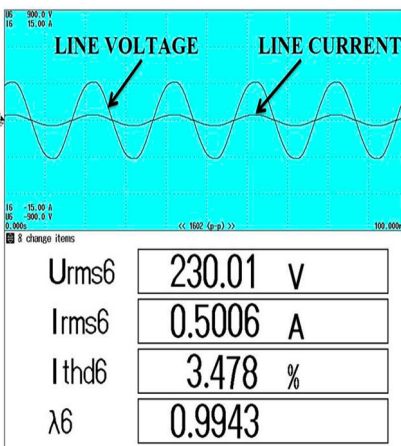
Figure 21. Hardware prototype for the modified converter.



(I)

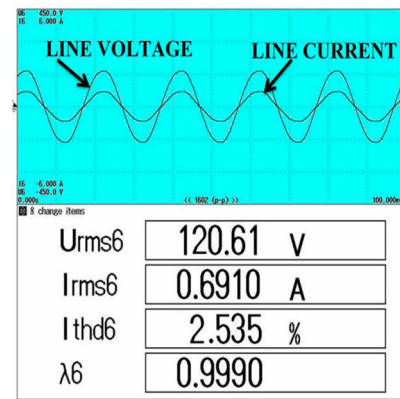


(II)

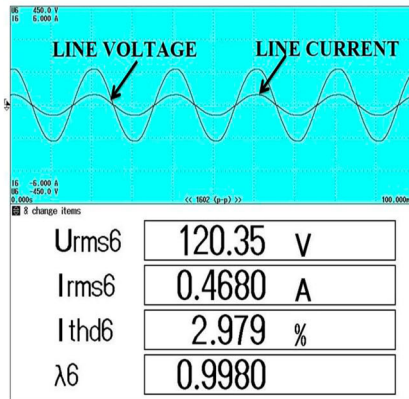


(III)

Figure 22. Functioning of the BMLCSC converter at the rated condition with (I–III) $V_{in} = 120, 170,$ and 230 V at $P_0 = 100$ W. Converter performance under 75% and 50% of load with (IV–V) $V_{in} = 120$ V.



(IV)



(V)

Figure 22. Continued.

Figure 22 (I–III) shows the experimental source voltage and current waveforms, including the corresponding THD and input power factor for variation in input voltage at 120, 170 and 230 V, respectively. The THD of the input current at 120, 170 and 230 V is 2.01%, 2.55%, and 3.47% also the input power factor close to unity. Figure 22 (IV–V) represents the input voltage and current waveforms with THD and power factor for load power variation under 75% and 50% at a source voltage of 120 V. The THD of input current at 75% and 50% of load is 2.53% and 2.97% with the input power factor maintained close to unity. The hardware outcomes are then validated with the recreation test results.

7. Comparison of BMLCSC converter with different converter topologies

Table 1 shows the comparison of the BMLCSC configuration to existing BL converter topologies. The preferred converter is good in the aspects of lesser components, higher efficiency, and better power quality. As a result, hence it is a viable low-cost PFC solution for arc welding power supplies.

8. Conclusion

The purpose of this research paper is to introduce a new configuration and shows the superiority of arc welding

Table 1. Modified converter and existing converter topologies.

S.No	Configurations	Number of Components					Total	Polarity of Output Voltage	Input Filter
		S	D	L	C				
1.	BL Cuk [21]	2	4	4	4	14	Negative	Yes	
2.	BL SEPIC [22]	2	4	4	3	13	Positive	Yes	
3.	BL Zeta [20]	2	4	4	3	13	Positive	Yes	
4.	BL Luo [24]	2	4	4	3	13	Negative	Yes	
5.	BL CSC [25]	2	4	2	3	11	Negative	Yes	
6.	BL Modified Landsman [27]	2	4	4	3	13	Negative	Yes	
7.	Proposed BMLCSC converter	2	2	3	3	10	Positive	No	

power supply applications. The circuit is simple and low-cost, when operated on DCM. The weeded topology lowered circuit components and elimination of the input filter. This DCM-based PFC converter supports augmented quality of power at the supply side and regulated load voltage at the output side for a wide range of load variations and supply voltage variations. The converter also managed to meet international PQ standards and the power factor is close to unity. According to the findings, the proposed converter outperforms in comparison with existing topologies. This modified bridgeless Landsman PFC converter possesses high efficiency around by 91.13%. Hence, the modified converter is well suited where high-quality weld beads requirements.

Disclosure statement

No potential conflict of interest was reported by the author(s).

ORCID

J. Gnanavadiivel  <http://orcid.org/0000-0002-9296-4370>

M. Shunmathi  <http://orcid.org/0000-0002-7375-7640>

References

- [1] Ramalho A, Santos TG, Bevans B, et al. Effect of contaminations on the acoustic emissions during wire and arc additive manufacturing of 316L stainless steel. *Addit Manuf.* 2022;51:102585.
- [2] Ke WC, Oliveira JP, Cong BQ, et al. Multi-layer deposition mechanism in ultra high-frequency pulsed wire arc additive manufacturing (WAAM) of NiTi shape memory alloys. *Addit Manuf.* 2022;50:102513.
- [3] Oliveira JP, Crispim B, Zeng Z, et al. Microstructure and mechanical properties of gas tungsten arc welded Cu-Al-Mn shape memory alloy rods. *J Mater Process Technol.* 2019;271:93–100.
- [4] Oliveira JP, Barbosa D, Fernandes FB, et al. Tungsten inert gas (TIG) welding of Ni-rich NiTi plates: functional behavior. *Smart Mater Struct.* 2016;25(3):03LT01.
- [5] Madhulingam T, Subbaiyan T, Shanmugam P, et al. Design and development of improved power quality based micro-butt welding power supply. *IET Power Electron.* 2017;10(7):746–755.
- [6] Arias Pérez de Azpeitia M, Vázquez Arduro A, Sebastián Zúñiga FJ. An overview of the ac-dc and dc-dc converters for LED lighting applications. *Automatika.* 2012;53(2):156–172.
- [7] Grigore V, Kyyra J. High power factor rectifier based on buck converter operating in discontinuous capacitor voltage mode. *IEEE Trans Power Electron.* 2000;15(6):1241–1249.
- [8] Rastogi SK, Rana MS, Mishra SK. A single-input multiple-output unity power factor rectifier. *IEEE Trans Power Electron.* 2020;36(9):10127–10141.
- [9] Henao GA, Castro JA, Trujillo CL, et al. Design and development of a LED driver prototype with a single-stage PFC and low current harmonic distortion. *IEEE Lat Am Trans.* 2017;15(8):1368–1375.
- [10] Shrivastava A, Singh B, Pal S. A novel wall-switched step-dimming concept in LED lighting systems using PFC zeta converter. *IEEE Trans Ind Electron.* 2015;62(10):6272–6283.
- [11] Durgadevi S, Umamaheswari MG. Analysis and design of single phase power factor correction with DC-DC SEPIC converter for fast dynamic response using genetic algorithm optimised PI controller. *IET Circuits Devices Syst.* 2018;12(2):164–174.
- [12] Singh S, Singh B. A voltage-controlled PFC Cuk converter-based PMBLDCM drive for air-conditioners. *IEEE Trans Ind Appl.* 2012;48(2):832–838.
- [13] Bist V, Singh B. A PFC-based BLDC motor drive using a canonical switching cell converter. *IEEE Trans Industr Inform.* 2014;10(2):1207–1215.
- [14] Singh PK, Singh B, Bist V. Brushless DC motor drive with power factor regulation using Landsman converter. *IET Power Electron.* 2016;9(5):900–910.
- [15] Jha A, Singh B. A PFC modified landsman converter-based PWM-dimmable RGB HB-LED driver for large area projection applications. *IEEE Trans Ind Appl.* 2017;53(2):1552–1561.
- [16] Singh PK, Singh B, Bist V. PFC converter based power quality improvement and ripple current minimization in BLDC motor drive. *IEEE International Conference on Power Systems*; 2016. p. 1–6.
- [17] Lin X, Wang F. A novel bridgeless buck PFC converter with half dead zones. *IEEE Conference on Industrial Electronics and Applications*; 2016. p. 602–606.
- [18] Jha A, Singh B. A bridgeless boost PFC converter fed LED driver for high power factor and low THD. *IEEMA Engineer Infinite Conference*; 2018. p. 1–6.
- [19] Son HS, Kim JK, Lee JB, et al. A new buck-boost converter with low-voltage stress and reduced conducting components. *IEEE Trans Ind Electron.* 2017;64(9):7030–7038.
- [20] Khan SA, Rahim NA, Bakar AA, et al. Single-phase bridgeless Zeta PFC converter with reduced conduction losses. *J Power Electron.* 2015;15(2):356–365.
- [21] Marimuthu G, Umamaheswari MG. Analysis and design of single stage bridgeless Cuk converter for current harmonics suppression using particle swarm optimization technique. *Electr Power Compon Syst.* 2019;47(11-12):1101–1115.

- [22] Jha A, Singh B. Bridgeless SEPIC PFC converter for multistring LED driver. *J Inst Eng India Ser B*. 2018;99(4):353–367.
- [23] Singh B, Bist V, Chandra A, et al. Power factor correction in bridgeless-Luo converter-fed BLDC motor drive. *IEEE Trans Ind Appl*. 2014;51(2):1179–1188.
- [24] Gnanavadiel J, Yogalakshmi P, Kumar NS, et al. Design and development of single phase AC–DC discontinuous conduction mode modified bridgeless positive output Luo converter for power quality improvement. *IET Power Electron*. 2019;12(11):2722–2730.
- [25] Singh B, Bist V. A BL-CSC converter fed BLDC motor drive with power factor correction. *IEEE Trans Ind Electron*. 2015;62(1):172–183.
- [26] Singh PK, Singh B, Bist V, et al. BLDC motor drive based on bridgeless landsman PFC converter with single sensor and reduced stress on power devices. *IEEE Trans Ind Appl*. 2017;54(1):625–635.
- [27] Kushwaha R, Singh B. Power factor improvement in modified bridgeless landsman converter fed EV battery charger. *IEEE Trans Veh Technol*. 2019;68(4):3325–3336.